Supporting Information

Dannemann et al. 10.1073/pnas.1719889115

SI Text

Basic Kinetic Equations. We subdivide the 2D space into a regular lattice of N square cells, the position of each cell center being labeled by a vector with integer components, $\mathbf{n} \in \mathbb{Z}^2$. The length of the cells is R_0, such that $R_0^2 = \pi R^2$, where R is the radius of the circular prey patches used in the simulations. This relation ensures that the area occupied by a prey patch is the same in simulations as in this theory. In addition, $R_0 \gg 1$, where the unit length represents the minimal distance that a predator can move during a displacement step. Only a subset of cells (patches) can contain prey, and for simplicity, such cells form a square sublattice with periodicity l_0, with l_0 being an integer > 1 (i.e., the patches have positions of the form $l_0\mathbf{n}$). Hence, the number of patches is $N_p = N/l_0^2$. Each prey patch can contain up to KR_0^2 prey, where K is the carrying capacity. In this space, predators perform independently random walk steps at a rate λ_0. The predator steps are continuous. The movements of the predators are described at the coarse-grained scale of the cells by a step probability distribution $P(\boldsymbol{\ell})$, where $\boldsymbol{\ell} = (\ell_x, \ell_y)$ is a displacement vector with integer components, like $\mathbf{n}$, describing the jump from one cell to another. We consider displacements with independent components drawn from the same distribution $p(n)$: $P(\boldsymbol{\ell}) = p(\ell_x)p(\ell_y)$, where

$$p(\ell) = p_0\delta_{\ell,0} + (1 - p_0)f(\ell). \qquad \textbf{[S1]}$$

The distribution $f(\ell)$ is normalized, such that $f(0) = 0$:

$$\sum_{\ell=\pm1,\pm2,\ldots} f(\ell) = 1. \qquad \textbf{[S2]}$$

From the above expressions, $p_0^2 = p(\ell = 0)^2$ represents the probability that the predator remains in the same cell after a move (when its actual step is too small to exit the cell).

We denote as $a_{\mathbf{n}}(t)$ and $b_{\mathbf{n}}(t)$ the densities of predators and prey in cell $\mathbf{n}$ at time t, respectively (the number of individuals in the cell divided by R_0^2). Prey are confined to their patches; thus, $b_{\mathbf{n}}$ is zero everywhere except if $\mathbf{n}$ is of the form $l_0\mathbf{m}$ with $\mathbf{m} \in \mathbb{Z}^2$. Assuming that the number of individuals in each occupied cell is large, we neglect stochastic fluctuations and write a deterministic rate equation for $a_{\mathbf{n}}$:

$$\frac{da_{\mathbf{n}}(t)}{dt} = -\lambda_0 a_{\mathbf{n}}(t) + \lambda_0 \sum_{\boldsymbol{\ell}} P(\boldsymbol{\ell}) a_{\mathbf{n}-\boldsymbol{\ell}}(t) + \lambda a_{\mathbf{n}}(t) b_{\mathbf{n}}(t) - \mu a_{\mathbf{n}}(t), \qquad \textbf{[S3]}$$

where λ and μ are the reproduction and mortality rates of the predator, respectively. The rate equation for $b_{\mathbf{n}}$ is

$$\frac{db_{\mathbf{n}}}{dt} = \sigma b_{\mathbf{n}} \left(1 - \frac{b_{\mathbf{n}} + a_{\mathbf{n}}}{K}\right) - \lambda' a_{\mathbf{n}} b_{\mathbf{n}}, \qquad \textbf{[S4]}$$

where σ is the prey reproductive rate and λ' is the predation rate. In Eq. **S4**, prey has a limited effective reproduction due to spatial constraints. In the corresponding stochastic lattice model exposed in the text, two individuals cannot occupy the same site. Prey will reproduce only if a randomly chosen neighboring site is empty, which occurs with probability $1 - (b_{\mathbf{n}} + a_{\mathbf{n}})/K$. To generate an offspring, a predator must encounter a prey, which occurs with probability proportional to $b_{\mathbf{n}}$. Therefore, predation is represented by the term $-\lambda' a_{\mathbf{n}} b_{\mathbf{n}}$ in Eq. **S4**, and predator reproduction is represented by $\lambda a_{\mathbf{n}} b_{\mathbf{n}}$ in Eq. **S3**.

Steady-State Solution. Because of their deterministic nature, the above equations are not appropriate to study patch extinction caused by demographic fluctuations. They are nevertheless useful as a first step to evaluate the average distribution of predators (and prey) in the system. We study the steady-state solutions of Eqs. **S3** and **S4** corresponding to species coexistence denoted as $a_{\mathbf{n}}$ and $b_{\mathbf{n}}$. Since prey patches are regularly spaced, we consider periodic solutions where the densities are the same in all prey patches, which we denote as $a_{l_0\mathbf{m}} = a_0$ and $b_{l_0\mathbf{m}} = b_0$. Setting the time derivatives to zero in Eq. **S4** and looking for nonvanishing solutions, we have, from **[S4]**,

$$b_0 = K - a_0(1 + K\lambda'/\sigma), \qquad \textbf{[S5]}$$

with a_0 yet to be determined. We introduce the discrete Fourier transforms

$$\hat{a}(\mathbf{k}) \equiv \sum_{\mathbf{n}} a_{\mathbf{n}} e^{-i\mathbf{k}\cdot\mathbf{n}}, \quad \hat{f}(\mathbf{k}) \equiv \sum_{\boldsymbol{\ell}} f(\boldsymbol{\ell}) e^{-i\mathbf{k}\cdot\boldsymbol{\ell}}. \qquad \textbf{[S6]}$$

The transform of Eq. **S3** leads to the stationary solution in Fourier space:

$$\hat{a}(\mathbf{k}) = \frac{\lambda a_0[K - a_0(1 + K\lambda'/\sigma)]}{\lambda_0[1 - \hat{P}(\mathbf{k})] + \mu} \sum_{\mathbf{n}} \cos(l_0\mathbf{k}\cdot\mathbf{n}), \qquad \textbf{[S7]}$$

where **[S5]** has been used. In **[S7]**, the sum has as many terms as the number of patches, and $\hat{P}(\mathbf{k})$ is the Fourier transform of the displacement distribution $P(\boldsymbol{\ell})$. The constant a_0 is obtained self-consistently from the inverse Fourier transform of $\hat{a}(\mathbf{k})$ evaluated at $\mathbf{n} = \mathbf{0}$:

$$a_0 = \frac{1}{(2\pi)^2} \int_{-\pi}^{\pi} dk_x \int_{-\pi}^{\pi} dk_y\, \hat{a}(\mathbf{k}) \equiv \frac{1}{(2\pi)^2} \int_{\mathcal{B}} d\mathbf{k}\, \hat{a}(\mathbf{k}), \qquad \textbf{[S8]}$$

where $\mathcal{B}$ denotes the first Brillouin zone of the square lattice. From **[S7]**, we obtain, apart from the trivial solution $a_0 = 0$,

$$a_0 = \frac{1}{1 + \frac{K\lambda'}{\sigma}} \left[K - \frac{1}{\frac{\lambda}{(2\pi)^2} \sum_{\mathbf{n}} \int_{\mathcal{B}} d\mathbf{k} \frac{\cos(l_0\mathbf{k}\cdot\mathbf{n})}{\lambda_0[1 - \hat{P}(\mathbf{k})] + \mu}}\right]. \qquad \textbf{[S9]}$$

Using the identity $\sum_{n=-M}^{M} e^{inx} = \sin[(M + 1/2)x]/\sin(x/2)$, one can also rewrite **[S9]** as

$$a_0 = \lim_{M\to\infty} \frac{1}{1 + \frac{K\lambda'}{\sigma}} \times \left[K - \frac{1}{\frac{\lambda}{(2\pi)^2} \int_{\mathcal{B}} \frac{dk_x\, dk_y}{\lambda_0[1 - \hat{P}(\mathbf{k})] + \mu} \frac{\sin[(M+1/2)l_0k_x] \sin[(M+1/2)l_0k_y]}{\sin(l_0k_x/2) \sin(l_0k_y/2)}}\right]. \qquad \textbf{[S10]}$$

Above, $(M + 1)^2$ is identified with the number of patches, and the limit is practically reached for $M \simeq 50$. From **[S1]**,

$$\hat{P}(\mathbf{k}) = [p_0 + (1 - p_0)\hat{f}(k_x)][p_0 + (1 - p_0)\hat{f}(k_y)]. \qquad \textbf{[S11]}$$

Inserting **[S9]** or **[S10]** into **[S7]** gives the full spatial distribution of predators in Fourier space. Of particular interest here is the total number of predators N_a in the system, which is directly deduced from the identity

$$N_a = R_0^2 \sum_{\mathbf{n}} a_{\mathbf{n}} = R_0^2 \hat{a}(\mathbf{k} = \mathbf{0}). \qquad \textbf{[S12]}$$

The spatially averaged predator density $a^* \equiv (\sum_{\mathbf{n}} a_{\mathbf{n}})/N = N_a/(NR_0^2)$ is also given by $N_a/(N_p l_0^2 R_0^2)$. Using **[S7]**, where the sum runs over the number of patches, and using the fact that $\hat{P}(\mathbf{k} = \mathbf{0}) = 1$ by normalization, one obtains

$$a^* = \frac{\lambda}{\mu l_0^2} a_0[K - a_0(1 + K\lambda'/\sigma)]. \qquad \textbf{[S13]}$$

Hence, the combination of Eqs. **S9** and **S13** gives the predator abundance. Similarly, the prey density in the patches, b_0, is readily obtained by combining Eq. **S5** with Eq. **S9**. In simulations, we computed the number of prey per unit area b^* (averaging over all sites, including empty ones). In the present theory, b^* is thus given by

$$b^* = \frac{b_0}{l_0^2} = \left(\frac{\lambda l_0^2}{(2\pi)^2} \sum_{\mathbf{n}} \int_B d\mathbf{k} \frac{\cos(l_0 \mathbf{k}\cdot\mathbf{n})}{\lambda_0[1-\hat{P}(\mathbf{k})]+\mu} \right)^{-1}. \quad \textbf{[S14]}$$

Predator Movements [p_0 and $f(\ell)$]. Before proceeding to an analysis of the above solution, we need to evaluate p_0. Consider predators that take random continuous displacement steps (l_x, l_y) with density distribution $p_s(l_x, l_y)$, such that the components l_x and l_y are independent and identically distributed:

$$p_s(l_x, l_y) = g(l_x)g(l_y). \quad \textbf{[S15]}$$

We also impose that $|l_x|$ and $|l_y|$ are larger than one (the minimal displacement length mentioned earlier), namely that $g(x) = 0$ for $|x| < 1$. Since there are no preferred directions, we take $g(x)$ as symmetric, $g(-x) = g(x)$, and given by the power law expression

$$g(x) = \frac{\beta-1}{2}|x|^{-\beta} \quad \text{for } |x|>1 \quad \textbf{[S16]}$$

$$= 0 \quad \text{for } |x|<1, \quad \textbf{[S17]}$$

where β is the exponent of the model. The above distribution is normalized to unity: $\int_{-\infty}^{\infty} dx\ g(x) = 1$. In this description, the long steps do not carry an additional time cost compared with short steps. We discuss in the last section the biological compatibility as well as the limitations of such an assumption.

To calculate p_0, we consider the 1D case, where cells are segments of length R_0, and assume that a walker that occupies a given segment can be anywhere inside it with uniform probability. The probability that a step does not bring the walker out of the segment is given by

$$p_0 = 2\int_0^{R_0} \frac{dr}{R_0} \int_0^r dx\ g(x) = \frac{2}{R_0}\int_1^{R_0} dr \int_1^r dx\ g(x), \quad \textbf{[S18]}$$

where the walker position has been averaged and the factor 2 takes into account left and right moves. We thus obtain

$$p_0 = 1 - \frac{1}{R_0} + \frac{1-R_0^{2-\beta}}{(2-\beta)R_0}. \quad \textbf{[S19]}$$

Therefore, the effect of the patch size is incorporated via p_0. When β is large (a random walk with jumps of unit length), $p_0 \simeq 1 - 2/R_0 \to 1$ at large R_0: only the predators that are close to the edges of the segment can exit in one step. Conversely, $p_0 \to 0$ as $\beta \to 1$, which is expected if the walkers nearly always take steps larger than R_0. We may extend the above arguments to calculate $p(\ell)$ for any integer ℓ. Instead, for simplicity, we will use from now on a power law form with integer argument for the normalized distribution function $f(\ell)$ appearing in Eq. **S1**:

$$f(\ell) = \frac{|\ell|^{-\beta}}{2\sum_{m=1}^{\infty} m^{-\beta}}, \quad \ell = \pm 1, \pm 2, \ldots \quad \textbf{[S20]}$$

Numerical Implementation.

Parameter values. In the numerical examples, we set $K = 1$. In the above analytic theory, the patches have a square shape, whereas they are circular in the stochastic simulations. To compare the two approaches, as mentioned in the first section above, we choose R_0, such that the patch areas are equal in both cases; that is,

$$R_0 = R\sqrt{\pi}, \quad \textbf{[S21]}$$

where R is the patch radius used in simulations. Substituting R by Eq. **8** (in scenario 1), one obtains

$$R_0 = \sqrt{\frac{\mu}{2n}}L, \quad \textbf{[S22]}$$

where n is the number of patches contained in the square simulation domain, which has $L \times L$ sites. In addition, we require that the distance between two neighboring patch centers in the analytic theory ($R_0 l_0$) is equal to the mean distance between neighboring patches in simulations ($L/\sqrt{n}$). In other words, the patch density is the same in both systems, which implies that

$$l_0 = \sqrt{\frac{2}{\mu}}. \quad \textbf{[S23]}$$

Recalling that l_0 is an integer, we round off this value. Therefore, for the results displayed in Fig. 5, the parameters are

$$\begin{aligned} &\mu = 0.05, \quad R_0 = 7.07, \quad l_0 = 7 \\ &\mu = 0.11, \quad R_0 = 10.48, \quad l_0 = 4 \\ &\mu = 0.20, \quad R_0 = 14.14, \quad l_0 = 3, \end{aligned} \quad \textbf{[S24]}$$

with $L = 500$ and $n = 125$ in all cases. For the theoretical results reported in Fig. 6*B*, one has used $L = 200$, $\mu = 0.05$ and $R_0 = 7.07$, and the other parameters are

$$\begin{aligned} &n = 5, \quad l_0 = 13 \\ &n = 40, \quad l_0 = 5 \\ &n = 80, \quad l_0 = 3. \end{aligned} \quad \textbf{[S25]}$$

Theoretical prey curves (Fig. 5, Lower). The theoretical prey density (averaged over space) is obtained by using Eq. **S14**. The fraction of area covered by the prey patches is chosen such that predators go extinct in scenario 1 when $\beta \sim 1$ (in the text and the section below on the MF approximation). Therefore, by decreasing β, the predator density decreases and vanishes at some point. At this same point, the prey density reaches its maximum carrying capacity value, $b_0 = K$, or

$$b^* = \mathcal{A}_{theor} \times b_0 = \frac{K}{l_0^2}, \quad \textbf{[S26]}$$

where $\mathcal{A}_{theor}$ is the fraction of area covered by the patches in the analytic model (that is to say, the fraction of cells that are patches). In simulations, patches are not regularly spaced but randomly distributed in space. Therefore, some overlap can exist between them, resulting in $\mathcal{A}_{simul} < \mathcal{A}_{theor}$, despite of the fact that the area of a patch and the number of patches per unit area are set equal in both models. Consequently, the resulting maximal prey abundance (b^*) will be overestimated in theory compared with simulations. For easier comparison, we have rescaled the theoretical curves of b^* as a function of β by the factor $\mathcal{A}_{simul}/\mathcal{A}_{theor}$, so that the spatially averaged carrying capacities of both systems are equal in the absence of predators. Hence, the theoretical and simulation curves of b^* start at the same point at small β in scenario 1 (Fig. 5, *Lower*).

Discretization and number of patches. To calculate the Fourier integrals, we resort to the approximation

$$\frac{1}{(2\pi)^2}\int_{\mathcal{B}} dk_x\, dk_y \to \frac{1}{N^2}\sum_{n_x=-N'}^{N'}\sum_{n_y=-N'}^{N'}, \quad \textbf{[S27]}$$

with $N = 2N' + 1$ and where the wave numbers have been discretized as $k_x = \frac{2\pi}{N} i$ and $k_y = \frac{2\pi}{N} j$ with i and j integers, respectively, comprised in $[-N', N']$. We consider a square regular domain of $2M \times 2M$ patches [with $M = 400$; that is to say, of $(2Ml_0)^2$ sites]. This value of M is used in Eq. **S9** or **S10**. This domain is itself embedded in a larger empty square lattice containing $N \times N$ sites. We choose $N = 2Ml_0 + 8000l_0$. This geometry is aimed at reducing errors due to the difficulty of evaluating

the Fourier integrals at small k when very large steps are frequent (limit β close to one; in the MF approximation section below).

Movement Strategy Maximizing a^*. We see that the spatially averaged density of predators a^* in Eq. **S13** obeys a logistic relation with respect to a_0, the density of predator in one prey patch. Thus, a^* is maximal when $a_0 = a_0^{(max)} \equiv K/[2(1 + K\lambda'/\sigma)]$, whereas it vanishes at $a_0 = 0$ and at $a_0 = K/(1 + K\lambda'/\sigma) = 2a_0^{(max)}$. In the low-density regime, $0 < a_0 < a_0^{(max)}$, the predators underexploit the patches (any increase in a_0 produces an increase of a^*), whereas for $a_0^{(max)} < a < 2a_0^{(max)}$, the high-density regime, the predators overexploit the patches (any increase in a_0 decreases the total abundance). Keeping all of the parameters of the model fixed except β, the density a_0 given by [**S9**] can be varied and tuned to $a_0^{(max)}$; thus, there should be a movement strategy that maximizes the whole-population abundance.

Through the parameter p_0 or λ_0, Eq. **S9** predicts that faster diffusion always results in a decrease of a_0. All of the other parameters being fixed, the largest possible value of a_0 is obtained in the absence of movement ($p_0 = 1$ or $\lambda_0 = 0$) and reads $a_0^{(no\ move)} = (K - \mu/\lambda)/(1 + K\lambda'/\sigma)$. Therefore, some amount of movement will increase the entire population if the latter value is located in the overexploitation regime or if $a_0^{(no\ move)} > a_0^{(max)}$, which implies that

$$\mu < \frac{K\lambda}{2}. \qquad \textbf{[S28]}$$

This condition is fulfilled in the simulations ($K = 1, \lambda = 1, \mu \ll 1$) and in the other cases considered here.

The optimal strategy is obtained by solving the equation $a_0 = a_0^{(max)}$, which gives, using Eq. **S9**,

$$\frac{1}{(2\pi)^2}\sum_{\mathbf{n}}\int_{\mathcal{B}} d\mathbf{k}\frac{\cos(l_0\mathbf{k}\cdot\mathbf{n})}{1-\hat{P}(\mathbf{k})+\mu^*} = \frac{2}{K\lambda^*}, \qquad \textbf{[S29]}$$

where

$$\mu^* = \frac{\mu}{\lambda_0} \quad \text{and} \quad \lambda^* = \frac{\lambda}{\lambda_0} \qquad \textbf{[S30]}$$

are the dimensionless mortality and reproductive rates (with respect to the movement rate), respectively. Mobile organisms typically have $\mu^* < K\lambda^* \ll 1$. To summarize, Eq. **S29** combined with Eqs. **S11**, **S19**, and **S20** gives the optimal β_c. Therefore, this exponent is a function of four variables and is not universal a priori: $\beta_c = \beta_c(\mu^*, K\lambda^*, R_0, l_0)$.

MF Approximation of the SLLVM. In the SLLVM studied in the paper, n patches of radius R are randomly distributed on a square lattice of length L. The carrying capacity is $K = 1$ for the sites belonging to the patches and $K = 0$ elsewhere. The fraction of area covered by the patches is given by $\mathcal{A}_{simul} \simeq n\pi R^2/L^2$ in simulations at small patch density (few overlap between patches) and by $\mathcal{A}_{theor} = 1/l_0^2$ in the analytic model. A simple MF solution of our SLLVM can be obtained when the predators are well-mixed across the system (i.e., in the random relocations regime or β close to one). Neglecting spatiotemporal fluctuations, we start from Eqs. **S3** and **S4**. In the MF approximation, $a_{\mathbf{n}}$ is uniform, independent of the cell position $\mathbf{n}$, and set to $a^{(MF)}$. A consequence of uniformity is the cancellation of the first two terms of the right-hand side of Eq. **S3** that describe movement fluxes. Denoting the prey density in a patch as $b_0^{(MF)}$, one obtains the following equations of evolution:

$$\frac{db_0^{(MF)}}{dt} = \sigma b_0^{(MF)}\left[1 - \frac{b_0^{(MF)} + a^{(MF)}}{K}\right] - \lambda' a^{(MF)} b_0^{(MF)} \qquad \textbf{[S31]}$$

$$\frac{da^{(MF)}}{dt} = \lambda b_0^{(MF)} a^{(MF)}\mathcal{A} - \mu a^{(MF)}. \qquad \textbf{[S32]}$$

The first equation is unchanged compared with Eq. **S4** for the prey density on a single patch. The second equation is like that of predators on a single prey patch in the absence of movement ($\lambda_0 = 0$), except that the reproduction term has been multiplied by $\mathcal{A}$. This is due to the fact that only the predators that occupy a patch (a fraction $\mathcal{A}$ of them) can reproduce and contribute to the growth of $a^{(MF)}$ in the whole system. The ordinary differential equations [**S31**] and [**S32**] yield an average predator abundance in the steady state given by

$$a^{(MF)} = \frac{K - \mu/(\mathcal{A}\lambda)}{1 + \lambda' K/\sigma}. \qquad \textbf{[S33]}$$

This expression is the same as Eq. **4** for $a_0^{(no\ move)}$, with λ substituted by $\mathcal{A}\lambda$. In scenario 1 of simulations, one chooses $\mathcal{A}$, such that predators go extinct in the well-mixed limit or $K - \mu/(\mathcal{A}\lambda) < 0$. In this case, only the trivial solution $a^{(MF)} = 0$ of Eq. **S32** is acceptable.

To show the consistency of our analytical results, the expression [**S33**] can be obtained in a different way by directly analyzing the full solution given by Eqs. **S9** and **S13** when β is close to unity. In this limit, the predator jump distribution is nearly uniform; therefore, its Fourier transform $\hat{P}(\mathbf{k})$ is very close to zero, except at small wave numbers, or $|\mathbf{k}| < 2\pi/L$, where $\hat{P}(\mathbf{k}) \simeq 1$. Therefore,

$$\frac{1}{(2\pi)^2}\sum_{\mathbf{n}}\int_B d\mathbf{k}\frac{\cos(l_0\mathbf{k}\cdot\mathbf{n})}{\lambda_0[1-\hat{P}(\mathbf{k})]+\mu} \simeq \frac{1}{L^2}\sum_{\mathbf{n}}\frac{1}{\mu} = \frac{1}{l_0^2\mu} = \frac{\mathcal{A}}{\mu}, \qquad \textbf{[S34]}$$

since the sum over $\mathbf{n}$ runs over patch cells. By substituting the above expression in Eq. **S9** and then in [**S13**], one recovers Eq. **S33**.

Time Costs and Velocity Assumptions in the Lévy Flight Model. Optimal foraging theory (OFT) assumes that an organism searching for resources makes behavioral choices in response to internal states and environmental factors and seeks to maximize the input gain while reducing energy expenditure. In fragmented environments, searching for patches that may be far apart is necessary. When facing predation risk and uncertainties regarding patch richness and local food availability (1, 2), a strategy that many organisms adopt is to increase travel velocity (3). This may incur an additional energetic cost, but it is part of the foraging trade-offs the organism faces while searching.

Consider the following examples. Bees tend to fly between patches with a certain speed, but when they need to travel to a distant spot, they increase their flying altitude to gain visual cues for orientation and then increase their flying velocity well above their normal one (4). Sharks, because of their anatomical design, must keep swimming continuously. A typical shark lower velocity is around 2 km/h, which is increased when a distant prey is detected, peaking at up to 40 km/h at the moment of the final chase and strike (5). Some birds may forage by jumping from gall to gall or from tree to tree (local searching) but travel at full velocity to distant areas (6). Finally, in the model studied in ref. 7 and inspired by herbivory mammals, foragers adopt a low velocity between local and nearby patches but increase their velocity with constant acceleration to reach distant patches. The velocity is bounded by a maximum value, which can be 10 times larger than the velocity used to explore nearby patches. Notice that, in such case, the notion of average velocity is not representative.

In all of the above examples, increasing velocity represents an effort to reduce traveling time, implying an energetic cost. Still, as said, this is a common foraging strategy that can be profitable.

This strategy may help to reduce the probability that a mobile prey—after it is spotted—may run away, or it may help to give a time advantage if another forager in the vicinity also spots the same target at the same time. When traveling to distant areas, this strategy also helps to increase dispersion and to reduce the time interval between feeding events (3) as well as the forager exposure time when not under vegetation covering (8).

When using a model where the forager moves following Lévy flights in a finite space (as is the case here), the time intervals are constant no matter the size of the jumps, which in turn, implies that the instant velocity is proportional to the jump length. Large jumps imply large velocities; hence, the Lévy flight model is in qualitative agreement with the observations mentioned above. Recall that, in Lévy flights, the scaling exponent is $1 < \beta < 3$. $\beta \sim 1$ corresponds to the regime where the forager travels with abundant large jumps. This will be the most energetically consuming strategy to follow (if the organism is not helped by air, water currents, or gravitational gradients). Additionally, our results point out that, with this strategy, the probability that the predator dies without descendency is high, because it misses many patches in the fragmented environment. However, a predator with $\beta \sim 3$ would move as a typical random walker with short steps having almost the same length. In this case, the predator velocity is low as is the energetic cost of moving. However, a population may go extinct if not finding a patch locally or by depleting the resources of a patch. Our results also suggest that a forager traveling with step lengths given by an intermediate β (close to two) will help maintain the stability of the ecosystem. In this scenario, high velocities are rare, while low velocities are the most frequent. Energetically speaking, this should be a good strategy for the predator to follow.

From the point of view of the OFT, which is concerned with energy balance and where time costs are important during foraging, the Lévy model is realistic up to a certain velocity scale. However, models such as Lévy walks with constant speed or Lévy walks with constant accelerations and a bounded velocity should be implemented in population models in the future.

1. Pitchford JW, et al. (2003) Optimal foraging in patchy turbulent environments. *Mar Ecol Prog Ser* 256:99–110.
2. Charalabidis A, et al. (2017) Risk of predation makes foragers less choosy about their food. *PLoS One* 12:e0187167.
3. Bartumeus F, et al. (2016) Foraging success under uncertainty: Search tradeoffs and optimal space use. *Ecol Lett* 19:1299–1313.
4. Esch H, Burns J (1996) Distance estimation by foraging honeybees. *J Exp Biol* 199:155–162.
5. Aidan MR, Hammerschlag N (2012) Marine predator–prey contests: Ambush and speed versus vigilance and agility. *Mar Biol Res* 8:90–94.
6. Houston AI (1986) The optimal flight velocity for a bird exploiting patches of food. *J Theor Biol* 119:345–362.
7. Shipley LA, et al. (1996) The dynamics and scaling of foraging velocity and encounter rate in mammalian herbivores. *Funct Ecol* 10:234–244.
8. Fewell JH (1988) Energetic and time costs of foraging in harvester ants, Pogonomyrmex occidentalis. *Behav Ecol Sociobiol* 22:401–408.

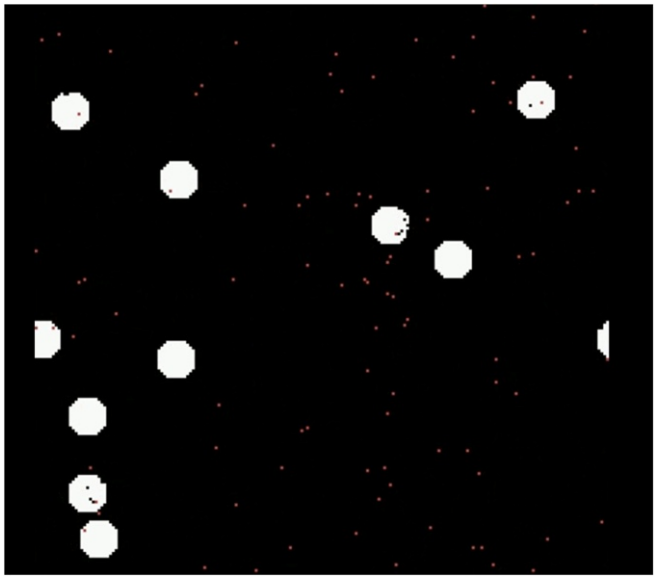

Movie S1. A simulation of the SLLVM. Predators (red dots) performing random relocations in the system ($\beta = 1.1$) go extinct over time due to underexploitation of the patchy prey (white dots).

Movie S1

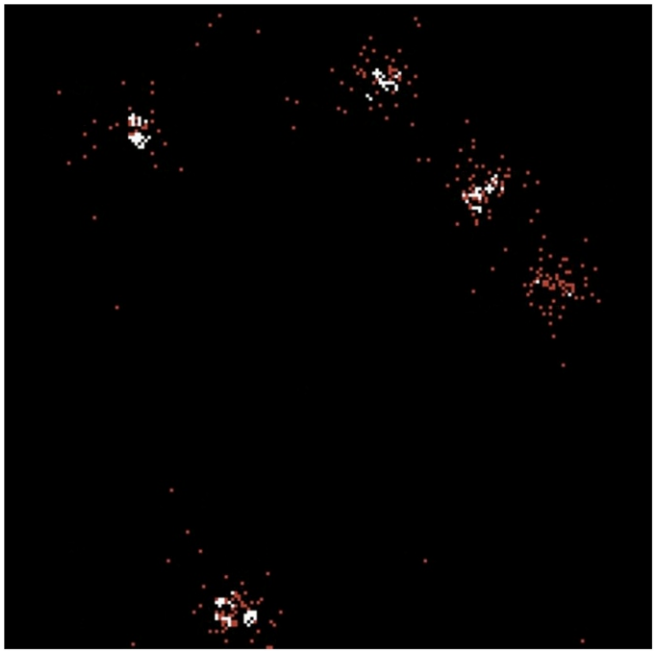

Movie S2. A simulation of the SLLVM. Both prey and predators (the latter performing Brownian random walks) go extinct due to patch overexploitation. The other parameters are the same as in Movie S1.

Movie S2

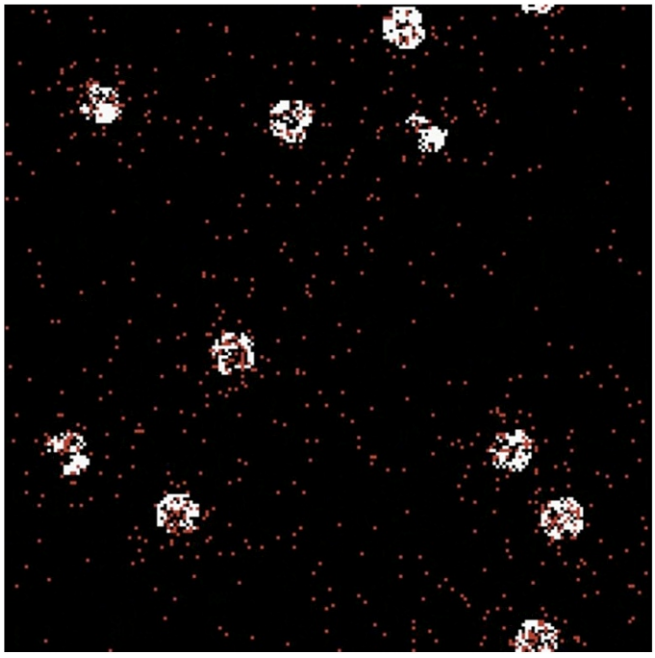

Movie S3. A simulation of the SLLVM with predators performing Lévy flights with $\beta = 2$. Prey and predators coexist, with the latter reaching high abundances. The other parameters are the same as in Movie S1.

Movie S3